THE ASTROPHYSICAL JOURNAL, 415:82–92, 1993 September 20

THE HIGHLY POLARIZED HIDDEN QUASAR IRAS 09104+4109: A DOUBLE-LOBED RADIO SOURCE IN A RICH CLUSTER

DEAN C. HINES[1] AND BEVERLEY J. WILLS[1]
Department of Astronomy and McDonald Observatory, University of Texas at Austin, Austin, TX 78712
Received 1992 October 29; accepted 1993 March 26

ABSTRACT

IRAS 09104+4109 is the second most luminous active galactic nucleus (AGN) so far discovered by *IRAS*, with $L_{bol} \sim 10^{12.6}\ h^{-2}\ L_\odot$. Kleinmann et al. have shown it to have a strong Seyfert 2 emission-line spectrum ($z = 0.442$), with a range of excitations and very large equivalent widths but no broad lines. They suggested that this $V \sim 19$ cD galaxy hides a luminous QSO that ionizes the narrow-line region and heats dust within $\sim$130 pc of the central engine. Here we further investigate the geometry and environment of this extreme AGN by means of broad-band polarimetry, spectropolarimetry, new spectroscopy, and radio imaging. The observed polarization is very high and strongly wavelength-dependent, increasing from 4% at 7500 Å to 21% at 3600 Å. The position angle is wavelength-independent with $\pm 5°$. The optical spectrum is dominated by unpolarized narrow-line emission and starlight. After correcting for dilution by these unpolarized components, we show that the remaining spectrum is highly polarized ($\sim$18%), and, within the uncertainties, this polarization is wavelength-independent. Spectrophotometry shows an ultraviolet excess and broad Mg II λ2798 emission that provide strong evidence that we are viewing a luminous quasar obscured in direct light but visible in light polarized by scattering. The polarization position angle is perpendicular to the position angle of an extended high-ionization [O III] emission region discovered by Kleinmann et al., so we postulate that this extended emission is ionized by the same collimated nuclear continuum source that gives rise to the scattered light. Assuming that the polarization arises in an optically thin scattering cone, we derive an opening angle less than 39° and inclination $\sim 35°$, and compare this geometry with the dust covering factor implied by the infrared luminosity.

If the observed wavelength dependence of polarization for IRAS 09104+4109 is typical of radio galaxies, it can explain the trend of increasing polarization with increasing redshift found by Tadhunter et al., strongly supporting their suggestion that this trend is the result of decreasing dilution of scattered light by unpolarized starlight, toward the shorter wavelengths.

IRAS 09104+4109 is also unusual in being the most powerful radio source associated with an *IRAS*-discovered object, and our new radio images show classic linear core and double-lobed structure. IRAS 09104+4109 is also a dominant cD galaxy in a rich, flattened galaxy cluster of intermediate redshift whose major axis is perpendicular to the radio jet. These facts suggest that this object may provide a clue to the relation between galaxy environment and strong radio jets.

Subject headings: galaxies: active — galaxies: clustering — galaxies: elliptical and lenticular, cD — galaxies: individual (IRAS 09104+4109) — quasars: general — polarization — radio continuum: galaxies

1. INTRODUCTION

IRAS 09104+4109 is the second most IR-luminous galaxy known, with $L = 6 \times 10^{12}\ L_\odot\ h^{-2}$ between 0.3 and 70 μm, of which 99% is emitted at wavelengths longer than 1 μm. It was found in a search for distant luminous galaxies (Kleinmann & Keel 1987) that selected *IRAS* sources strong at 60 μm (>0.5 Jy), with nonstellar colors $F(60\ \mu m)/F(25\ \mu m) < 3$, and with faint optical counterparts (>18 mag). Kleinmann et al. (1988, hereafter K88) identified IRAS 09104+4109 with a $V \sim 19$ cD radio galaxy near the center of a rich, flattened cluster at redshift 0.442. Their optical spectroscopy of the nucleus shows a characteristic Seyfert 2–type spectrum having strong, narrow emission lines with a range of ionizations, implying photoionization by a strong ultraviolet nonthermal continuum. However, no very broad lines were seen, not even in Hα. Thus they suggested that the strong infrared excess is produced by dust obscuring a QSO-like[2] broad-line region.

K88 also present *R*-band and narrow-band images. The [O III] $\lambda\lambda$4959, 5007 image is extended to the northeast in position angle $\approx 14°$. They suggest that the extended emission may be a remnant of a captured galaxy. Hutchings & Neff (1988) present a photometric *R*-band image taken in 0.″8–1.″2 seeing, and find "secondary nuclei" 3″ to the north and northeast of the nucleus, coincident with the extension in the [O III] image. They find no direct evidence that IRAS 09104+4109 is interacting or merging with the other galaxies in the field.

Motivated by the discovery of unusually high and wavelength-dependent optical-infrared polarization in the radio-quiet QSO IRAS 13349+2438 (Wills et al. 1992b), we have carried out an optical polarization survey of a sample of

[1] Guest observers, National Radio Astronomy Observatory, which is operated by Associated Universities, Inc., under cooperative agreement with the National Science Foundation.

[2] Here we use the term "QSO" to refer to very luminous AGNs in general, having $M_V < -21.5$, and "quasar" to refer to those that are radio-loud. We adopt a cosmology in which $H_0 = 100\ km\ s^{-1}\ Mpc^{-1}$ and $q_0 = 0.5$.

all *IRAS* ultraluminous active galactic nuclei (AGNs) known to us, with log $(L_{ir}/L_{\odot}) \geq 11.5$ and "warm" $[0.25 \leq F(60\ \mu m)/F(25\ \mu m) \leq 3]$ infrared colors. The main results will be presented elsewhere (Wills & Hines 1993), but here we present the results for IRAS 09104+4109 separately because of its very unusual properties.

Our optical broad-band polarimetry, spectropolarimetry, and new spectrophotometry observations, together with new radio continuum imaging, are described in § 2, and the results are presented in § 3. In § 4 we estimate the fraction of light contributed by the host galaxy, then correct the polarization for dilution by unpolarized emission lines and starlight. The polarization mechanism is discussed in § 5. In § 6 we discuss in more detail a model for IRAS 09104+4109 based on an interpretation in which a polarized ultraviolet spectrum arises from scattered QSO light. In § 7 we briefly compare the properties of IRAS 09104+4109 with those of other AGNs, from the point of view both of unifying models and of the evolution of cluster radio sources. Finally, in § 8, we summarize our conclusions.

2. OBSERVATIONS

Table 1 gives a log of the observations. In the following sections we give further details.

2.1. *Broad-Band Linear Optical Polarimetry*

Our broad-band optical polarization measurements were made with the polarimeter described by Breger (1979), mounted at the f/13.6 Cassegrain focus of the 2.1 m Struve telescope of McDonald Observatory. The detector was a cooled (−20°C) Hamamatsu R943-02 phototube [GaAs(Cs) photocathode] operated in photo-counting mode. We observed IRAS 09104+4109 on UT 1989 January 12 in white light (no filter) and found it to be significantly polarized ($p = 9.1\% \pm 1.6\%, \theta = 95° \pm 5°$). We then observed the object with *UBVRI*, $CuSO_4$, and RG630 filters to look for wavelength dependence.

Normally, a Lyot depolarizer is used in the optical train after the rotating Glan prism to eliminate the effects of polarization sensitivity of the succeeding optical elements and the photocathode, but this type of depolarizer is only effective over fairly large bandwidths (>100 Å). Since the spectrum of IRAS 09104+4109 is dominated by very strong narrow emission lines, the measurements were made without the depolarizer for the *V*, *R*, and *I* filters. Instrumental polarization was measured by observing null standards, while the absolute position angle was calibrated using observations of polarized standard stars (Hsu & Breger 1982). The typical instrumental polarization was $p \approx 0.06\%$ with the Lyot depolarizer and $p \approx 2.1\%$ without it.

All observations were made using a projected aperture diameter of 5".2, except for the *V* and *R* filters, where a 10" aperture was used. Conditions during all observations were photometric, with seeing ~2". A more detailed description of the data reduction procedure can be found in Wills et al. (1992a).

2.2. *Spectophotometry and Spectropolarimetry*

The spectrophotometry and spectropolarimetry were obtained using the Large Cassegrain Spectrograph (LCS) at the f/17.8 Cassegrain focus of the McDonald Observatory 2.7 m telescope.

The spectrophotometry was obtained with a 300 line mm^{-1} grating and an east-west slit of width 10". The detector was a thinned 800 × 800 TI CCD, giving a reciprocal dispersion of 3.45 Å per pixel. The sky was clear, but the seeing was poor, ~4"–7". The object spectra were extracted using a 12" box and the sky extracted in ~10" windows on either side. Flux calibration was by means of observations of spectrophotometric

TABLE 1

LOG OF OBSERVATIONS

Instrument	Band	Aperture (")	Seeing (")	Integration (seconds)	UT Date
Breger Polarimeter[a]	*U*	5.2	2	1200	1989 Feb 4
	B	5.2	1	1400	1989 Apr 7
	$CuSO_4$	5.2	2.5	800	1989 Jan 12
	$CuSO_4$	5.2	3	400	1989 Jan 14
	$CuSO_4$	5.2	2	1200	1989 Feb 4
	V	10.4	2	1800	1989 Apr 8
	"open"	5.2	2.5	400	1989 Jan 12
	R	5.2	1	1000	1989 Apr 7
	RG630	5.2	3	800	1989 Jan 14
	RG630	5.2	2	900	1989 Feb 4
	I	10.4	2	1400	1989 Apr 8
LCS[b]	3170 – 5885Å	10×130[c]	4	3600	1990 Jan 25
LCS/Spectropolarimeter[b]	5187 – 7908Å	2×64[c]	2	7200	1991 Jan 13
	5197 – 7922Å	2×64	4	7200	1991 Mar 16
	5197 – 7922Å	2×64	2	7200	1991 Mar 18
VLA (C-array)	6cm (5 GHz)	4.7[d]	...	9000	1989 Jul 15
VLA (A-array)	20cm (1.4 GHz)	1.4[d]	...	14400	1990 Apr 10

[a] At the f/13.6 Cassegrain focus of the 2.1 m Struve telescope of McDonald Observatory.
[b] At the f/17.8 Cassegrain focus of the 2.7 m telescope of McDonald Observatory.
[c] The object spectra for both the spectrophotometry and the spectropolarimetry were extracted with a 12" box aperture.
[d] Full width at half-maximum, natural-weighted, circular beam size.

standards from Stone (1977). The accuracy of our relative flux densities is ~5%.

The LCS was used for spectropolarimetry with a setup like that for spectrophotometry, but with polarimeter optics as described by Goodrich (1991) and a 2″ × 64″ east-west slit. The sky was hazy except for UT 1992 March 16, which was photometric. The dual-beam design of the spectropolarimeter ensures accurate polarimetry even in nonphotometric conditions (Miller, Robinson, & Goodrich 1988). Instrumental polarization was measured, and absolute polarization was calibrated, by observing unpolarized and polarized standard stars. The instrumental polarization was negligible (<0.1%), and the absolute position angle is accurate to within 2°. In addition to the polarized standards, we observed several polarized objects before and after the observations of IRAS 09104+4109. These additional observations were consistent with previous broad-band polarization measurements, so we are confident of the correctness of our measurements. The flux density calibrations and extraction of spectra were done in the same way as for the spectrophotometry. Within a spectrum the accuracy of the flux density calibration is ~5%, while slit losses render the absolute calibration of the nuclear flux accurate to ~20%. A more detailed discussion of the observing procedures and data reduction will be presented in a later paper (Hines & Wills 1993).

2.3. *Radio Continuum Observations*

We observed IRAS 09104+4109 at 6 and 20 cm using the Very Large Array (VLA)[3] with the C- and A-arrays (Table 1), for 2.5 hr on UT 1989 July 15 and 4 hr on UT 1990 April 10, respectively. The data were reduced using the calibration and imaging packages in AIPS. The absolute flux density scale was based on flux densities for the primary calibrator 3C 286 provided in the AIPS 1990 July 15 package, and the phases were calibrated using observations of 3C 147. We observed 3C 286 for 10 minutes at the beginning of the observing sessions, and 3C 147 for 5 minutes every 15 minutes. The final images were produced using natural weighting in the *uv* plane, giving effective half-power beamwidths of 4.″7 and 1.″4 at 6 and 10 cm, respectively. For both images the off-source rms noise is ≈32 μJy beam^{-1}.

3. RESULTS

The important observational results are the strong wavelength-dependent polarization and the polarization position-angle alignment (discussed in § 6.1), the ultraviolet excess and broad Mg II λ2798 emission line, and the lack of polarization in the strong narrow-line spectrum. Each is discussed in more detail below.

3.1. *Broad-Band Polarimetry*

One of the most striking results is presented in Table 2 and in Figure 1. We find unusually high and wavelength-dependent broad-band polarization, rising from ~4% at 7500 Å to 21% at 3600 Å. The position angle, ~97°, is wavelength-independent within the observational uncertainties of ~5°,

[3] The Very Large Array is operated by the National Radio Astronomy Observatory for Associated Universities, Inc., under contract with the National Science Foundation.

TABLE 2

POLARIZATION RESULTS FOR IRAS 09104+4109

Band	λ[a] (Å)	p (%)	σ_p (%)	p_{deb}[b] (%)	θ (°)	σ_θ (°)	p_{cor}[c] (%)	p_{cor}[d] (%)
U	3600	21.0	±3.2	20.7	100	±5	...	...
B	4200	14.8	2.6	14.6	109	5	16.2	16.8
$CuSO_4$	(4800)	11.7	1.1	11.6	100	3	...	...
V	5300	10.2	2.3	10.0	90	6	12.8	20.2
"open"	(5700)	9.1	1.6	9.0	95	5	...	...
[OIII]	7151	0.9	0.4	1.6[e]	171	...	...	...
R	7200	4.8	1.0	4.6	104	6	12.6	21.0
[OIII]	7220	0.3	0.1	0.5[e]	100	8	...	...
RG630	(7500)	4.2	0.6	4.1	84	4	...	...
I	7900	5.1	2.9	4.2	97	...	7.7	17.4

[a] Approximate observed effective wavelength for the filter bandpass (for the polarization before dilution correction in the case of broad-band data).

[b] Debiased percentage polarization using the method in Wardle & Kronberg 1974.

[c] Percentage polarization corrected for the unpolarized narrow emission lines (assumed unpolarized).

[d] Percentage polarization corrected for dilution by the narrow emission lines and galaxy starlight.

[e] Upper limit to the percentage polarization corresponding to the 95% confidence interval, derived using the Rice distribution (Fig. 5 of Simmons & Stewart 1985).

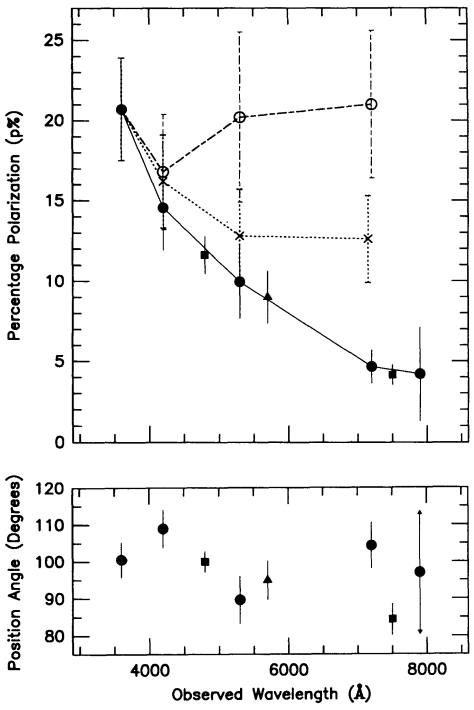

FIG. 1.—Broad-band polarization results. Filled symbols represent the observed filter polarizations: circles are the *UBVRI* filters, the triangle is the "open" filter, and squares represent the $CuSO_4$ and RG630 filters. Crosses represent the polarizations corrected for dilution by the unpolarized narrow emission lines, and open circles represent the polarizations corrected for dilution by the unpolarized narrow emission lines and the stellar continuum (see text). The observed polarizations have been bias-corrected using the prescription of Wardle & Kronberg (1974). Error bars represent the 1 σ errors based on pure photon-counting statistics. The errors in position angle are also 1 σ errors except for the *I*-band errors, which are not well defined because of the low significance of the measurement. These errors do not include the ±2° error in absolute position-angle calibration.

and the rotation between rest wavelengths of 2400 and 5200 Å is probably less than 10°. This polarization is a property of the continuum only, as the strong [O III] emission lines are essentially unpolarized (§ 3.3).

In Table 2, column (1) gives the filter used, column (2) the approximate effective wavelength of the filter, column (3) the percentage polarization, column (4) the 1 σ error in the polarization (based on photon statistics, which is the dominant uncertainty), column (5) the estimated polarization after bias correction using the method of Wardle & Kronberg (1974), columns (6) and (7) the polarization position angle and its 1 σ error, column (8) the polarization corrected for dilution by emission lines, and column (9) the polarization corrected for dilution by emission lines and starlight (§ 4). For all plots and calculations, we use the debiased polarizations $p_{\rm deb}$. We find the effective wavelength for which the measured polarization occurs by integrating the expected count rates for polarized and total light across the bandpass. These expected wavelength-dependent count rates are determined by multiplying the best estimates of polarized or total photon flux densities by the cataloged transmission for the V filter and the measured transmissions for the R- and I-band filters, the manufacturer's response for the Hamamatsu phototube, and standard atmospheric transmission for McDonald Observatory. The best estimates of the photon spectra are taken from spectrophotometry (see below), assuming that the percentage polarization across the bandpass can be interpolated from the broad-band polarization measurements. The effective wavelength is then the wavelength at which the derived degree of polarization is equal to the "model" polarization.

3.2. *Spectrophotometry*

Figure 2 shows the rich emission-line spectrum between rest wavelengths of 2160 and 6200 Å. Our data have been scaled to match the redder spectrophotometric data of K88, using the region of overlap between rest wavelengths of 3232 and 4023 Å. The equivalent widths of [Ne V] λ3426 agree to within 5%. However, in our scaled spectrum, we measure 14% more flux in the [O II] λ3727 line than K88 do, consistent with extended [O II] emission contributing more to the flux in our larger effective aperture.

There is a clear dip in the spectrum at the expected wavelength of the 4000 Å break (Fig. 2, *middle panel*). Below 3300 Å rest wavelength the spectrum is dominated by a UV excess relative to that expected for a typical elliptical galaxy (K88).

Another important result is the detection of a broad component of Mg II λ2798. Using the narrow Hβ line as a template, we subtracted the narrow-line contribution of the Mg II doublet. Gaussian fitting to the remaining broad component yielded a line width (FWHM) of 10,000 $\pm$ 1000 km s^{-1} and rest-frame equivalent width of 38 $\pm$ 7 Å. This equivalent width is typical of low-redshift quasars when measured with a similar choice of continuum (Grandi 1981). There is no sign of broad Hβ, although its detection is made very difficult by the presence of (uncorrected) atmospheric B-band absorption and the great strength of the Hβ and [O III] narrow-line emission.

3.3. *Spectropolarimetry*

Figure 3 shows the results of our spectropolarimetry. The top panel gives the total flux spectrum F_λ; the middle panel gives the rotated Stokes parameter, $\mathrm{RSP}_\lambda = q \cos 2\theta + u \sin 2\theta$, where the polarization position angle, $\theta = 102°$, is determined directly from our spectropolarimetry;[4] and the bottom panel gives the Stokes flux, $\mathrm{SF}_\lambda = \mathrm{RSP}_\lambda \times F_\lambda$. We present RSP_λ and SF_λ because, unlike the percentage polarization and the polarized flux, they do not suffer from the biased statistics that affect data at low signal-to-noise ratios. The noise can thus be estimated directly from the plots. *Clearly, the* [O III] *emission is of very low polarization, perhaps unpolarized, and the other narrow emission lines, including* Hβ, *are probably unpolarized as well.* This is consistent with the apparent lack of reddening of the narrow-line spectrum noted by K88. For the [O III] lines alone we measure $p(\lambda 5007) = 0.3\% \pm 0.1\%$ and $p(\lambda 4959) = 0.9\% \pm 0.4\%$.

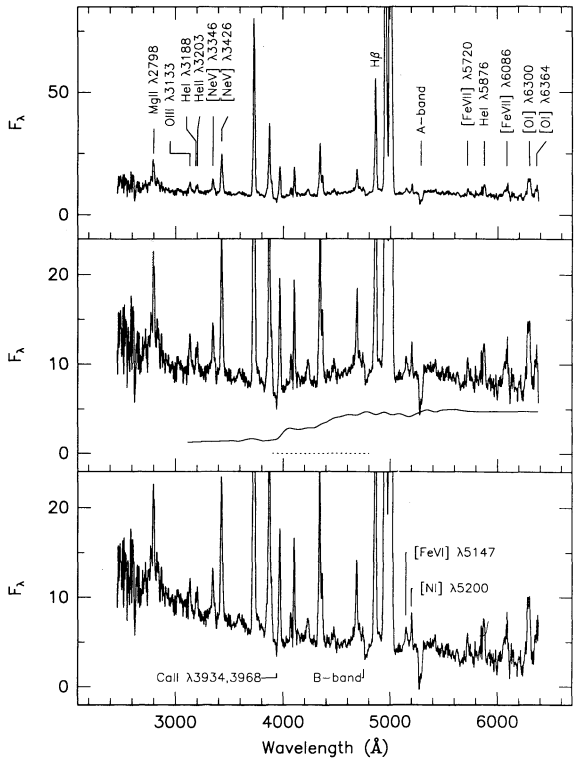

FIG. 2.—Spectrum of IRAS 09104+4109 and the contribution from the host-galaxy starlight. The ordinate gives observed flux densities in units of 10^{-17} ergs s^{-1} cm^{-2} Å^{-1}, and the abscissa gives rest-frame wavelengths ($z = 0.442$). The top panel shows our blue spectrum combined with the redder spectrum of K88. Some unmarked lines are marked in Fig. 3. The middle panel gives an expanded view of the spectrum and shows the contribution of starlight estimated by scaling an E/S0 galaxy spectral energy distribution (Wells 1978) to match the continuum shape in the 4000–5000 Å region (*dotted line*). The bottom panel gives the galaxy-subtracted spectrum.

The negligible polarization of the narrow emission lines indicates that any contribution to the polarization by transmission trough the interstellar medium of our Galaxy or the host galaxy of IRAS 09104+4109 is less than 0.7%, consistent with the maximum expected contribution from our Galaxy in the direction of IRAS 09104+4109 ($l = 181°$, $b = +44°$)—less than 0.1%. This latter limit is based on $E(B-V) < 0.01$ (Burstein & Heiles 1982) and the empirical relation $p_{\rm isp} \leq 9E(B-V)\%$ (Serkowski, Mathewson, & Ford 1975).

[4] We tested the validity of this assumed θ by comparing the Stokes flux for various angles between 0° and 180° in 10° steps. There was no significant Stokes flux in the regions of the emission lines for any θ, but the continuum SF_λ did peak at $\theta \sim 102°$.

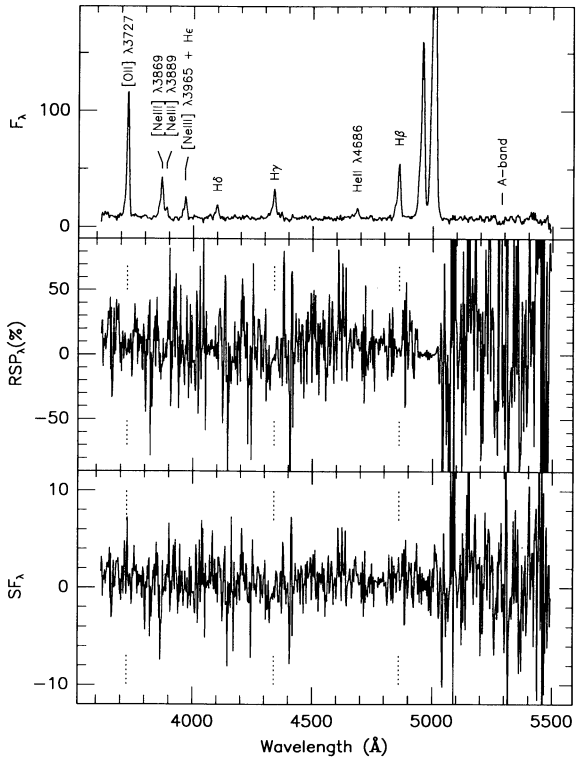

FIG. 3.—Spectropolarimetry results for IRAS 09104+4109. The flux densities (F_λ and SF$_\lambda$) and wavelengths are in the same units as in Fig. 2. The top panel gives the total flux spectrum, the middle panel gives the rotated Stokes parameter (in percent), and the bottom panel gives the Stokes flux. The vertical dotted lines in the two lower panels indicate the wavelengths of strong emission lines (see top panel). Note that, at the wavelengths of the strong emission lines, RSP$_\lambda \approx 0\%$, and no excess polarized flux is present. This indicates that the strong emission lines, and probably all narrow emission lines, are unpolarized.

3.4. *The Radio Image*

Our radio images at 20 cm (Fig. 4) and 6 cm show classic core and double-lobed structure.[5] At 6 cm K88 detected the compact core and the north-preceding (Np) lobe. The emission that they found between these components is almost certainly real, and our 20 cm image shows it clearly as a connecting bridge. The linear "jets" (or perhaps bridges) have a well-defined position angle of 333° (153° for the south-following [Sf] lobe). Table 3 gives the measured flux densities and approximate spectral indices for various features in the 6 and 20 cm images. Since we obtained the 6 cm data with the C-array and the 20 cm data with the A-array, we may underestimate the flux densities for the extended lobe emission at 20 cm due to lack of short spacings, but not at 6 cm. So the true spectral indices could be steeper, but are unlikely to be flatter than we have derived. We note that the total flux densities for the core agree with the values in K88. The total radio power at 1.4 GHz (20 cm) ($P_{1.4} = 3.2 \times 10^{24}$ W Hz^{-1}) places IRAS 09104+4109 near the break between Fanaroff-Riley I (FR I) and the more powerful FR II radio sources (e.g., Bridle & Perley 1984), and the ratio of core to lobe flux density [R(1.4 GHz) $\approx$ 1 in the rest frame] is quite large for such a linear and symmetric morphology. The radio structure is somewhat anomalous, and the possible significance of this is discussed further in § 7.2.

[5] We do not show the 6 cm image, since the resolution is much lower and reveals no additional interesting structure.

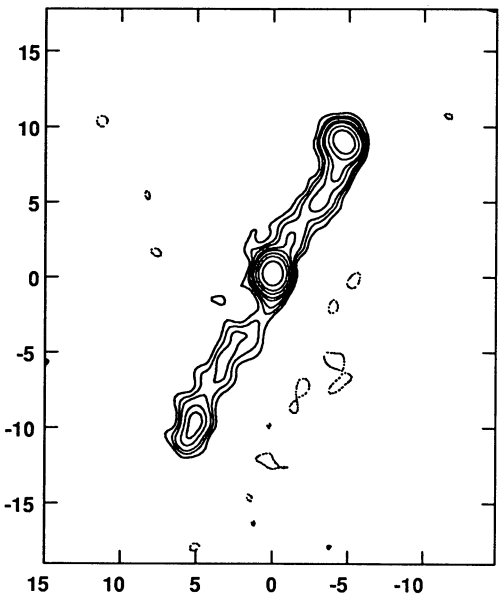

FIG. 4.—The 20 cm radio image (north is at the top, and east is to the left). The axes show the offset (in arcseconds) from the optical position measured with the UTRAO measuring engine at the University of Texas (R.A. = 09^{h}10^{m}32^s.86, declination = 41°08′53″.2 [1950.0]). This optical position agrees to within 0″.5 of the "deconvolved," central-peak 20 cm flux density. The contours are −3, 3, 5, 7, 11, 15, 25, 40, and 74 times the off-source rms noise (31 μJy beam^{-1}). The beam is ≈1″.4 × 1″.3 at a position angle of 13° and is given approximately by the 74 contour. The peak flux density is 4.56 mJy beam^{-1}.

4. CORRECTION OF THE NUCLEAR SPECTRUM FOR UNPOLARIZED EMISSION LINES AND STARLIGHT

The presence of a 4000 Å break and strong Ca II K absorption in the nuclear spectrum of IRAS 09104+4109 (Fig. 2 and K88), as well as the extended optical morphology, show that starlight is an important component of the spectrum. In order to isolate the nuclear spectrum, including the polarized component, we need to correct our observed spectra and polarization for dilution by the strong unpolarized emission lines and starlight within our observing apertures. The starlight is assumed to be unpolarized because it is the integrated light of stars over most of the host galaxy.

We have modeled the stellar emission of IRAS 09104+4109 using the average optical E/S0 galaxy spectral energy distribution given by Wells (1978), scaled to match the strength of the 4000 Å break and the shape of the stellar continuum between about 4000 and 5000 Å. We chose to match this region because it is the most reliable indicator of the amount of starlight. At least 50% of the emission longward of ~4500 Å (rest frame) is

TABLE 3

RADIO FLUX DENSITIES

Feature	S_ν(6 cm) (mJy)	S_ν(20 cm) (mJy)	α[a]
Np hot spot	0.8	3.3	−1.2
Np lobe	0.8	5.6	−1.5
Core	1.6	5.9	−1.0
Sf lobe	0.2	2.7	−2.2
Sf hot spot	<0.1	1.4	< −2.3
Total	2.5	14.3	−1.4

[a] $S_\nu \propto \nu^\alpha$.

starlight. Figure 2 illustrates the modeling: the top panel shows the rest-frame total flux spectrum derived by combining our blue spectrum with the red spectrum from K88, the middle panel gives both the total flux spectrum and the model galaxy continuum with the region of fit given by the dashed line, and the bottom panel gives the model-subtracted spectrum. We estimate $\pm 30\%$ uncertainty in the flux contribution of the galaxy starlight.

Between rest wavelengths of 3200 and 6000 Å the galaxy-subtracted continuum can be fitted by a power law, $F_\nu \propto \nu^{-0.6}$. K88 also note this excess emission at rest wavelengths between 3000 and 4000 Å compared with the normal stellar component found in many elliptical galaxies—a situation similar to that seen in Seyfert galaxies. This excess could arise from a recent burst of star formation or scattered light from a hidden AGN (§ 5.3, 6).

Because the continuum is faint, its polarization is much better determined by the broad-band data than by the spectropolarimetry; but it must be corrected for dilution by the unpolarized emission. We first correct for the emission lines alone, and then for the unpolarized starlight as follows.

In general, we begin with a model for p_λ interpolated from the observed broad-band values, the unpolarized diluting spectrum $F_{\lambda,d}$, and the total flux density spectrum F_λ derived from spectrophotometry. We derive the pure polarized flux spectrum $P_\lambda = p_\lambda F_\lambda$. P_λ, F_λ, and $F_{\lambda,d}$, are corrected to instrumental fluxes by correcting the corresponding photon flux densities for atmospheric transmission, filter transmission, and photocathode response (§ 3.1). These are converted to instrumental count rates by integration over the passband of the filter under consideration to derive $\boldsymbol{P}$, $\boldsymbol{F}$, and $\boldsymbol{F_d}$. A better estimate of the continuum polarization is then $\boldsymbol{P}/(\boldsymbol{F} - \boldsymbol{F_d})$ at an effective wavelength corresponding to this continuum polarization in the model. This can be iterated with the new improved model for p_λ over the appropriate passband. In practice, no iteration was really needed. In making the first correction, for emission lines alone, we have used a spline fit through the observed continuum to isolate the diluting emission-line spectrum. The second correction, for galaxy starlight dilution, is particularly simple because the first iteration leads to an essentially wavelength-independent degree of polarization.

The dilution-corrected polarizations for the I, R, V, and B bands are given in Table 2 and are plotted in Figure 1 as crosses (corrected for emission lines) and as open circles (corrected for emission lines and starlight). The errors were determined by scaling the observational (1 σ) errors by the dilution correction factors. The resulting dilution-corrected polarization is, within the uncertainties, wavelength-independent. Assuming that the deviations from constant polarization are caused by random errors only, the error-weighted, dilution-corrected polarization is $\langle p \rangle \approx 18\%$.

5. THE POLARIZATION MECHANISM

Polarizations of order 20% are uncommon in high-luminosity AGNs, except for the blazars (e.g., Martin et al. 1983; Stockman, Moore, & Angel 1984; Thompson & Martin 1988; Brindle et al. 1990a, b). The high polarization of IRAS 09104+4109 and the likely wavelength independence of position angle suggests that one polarization mechanism is dominant, which simplifies the following discussion. The lack of polarization of the strong emission lines shows that the polarization is generated within narrow-line region (NLR) distances of the nucleus. We consider three possible mechanisms independently.

5.1. *Dichroic Transmission*

After correction for dilution by unpolarized light, the polarization spectrum of the nuclear continuum is too uncertain to exclude the characteristic wavelength dependence expected for dichoric transmission, i.e., transmission through aligned grains as for normal interstellar polarization in our Galaxy (Whittet et al. 1992). While this mechanism could operate within NLR distances of the nucleus of IRAS 09104+4109, the observed high polarization would require an unusually high degree of grain alignment. If this mechanism operates, further investigation could lead to an understanding of magnetic fields near the central engine.

5.2. *Synchrotron Emission*

Synchrotron emission can produce a very high degree of wavelength-independent polarization that is usually highly variable, as in the highly polarized quasars (HPQs; Stockman et al. 1984). Impey, Lawrence, & Tapia (1991) and Wills et al. (1992a) find that the probability of high, variable optical polarization is a strong function of R (the ratio of core to lobe flux density), such that objects with $\log R < 0$ are rarely polarized (Fig. 2*b* of Wills et al.). Based on observed ratios of radio core to optical flux densities for the synchrotron spectra of high-R quasars, corresponding to α(radio-opt) ~ -0.7, the optical flux corresponding to the 5 GHz 1.6 mJy core of IRAS 09104+4109 would probably be less than 0.6% of the flux at any optical band. Therefore, we would not expect significant optical synchrotron polarization in IRAS 09104+4109.

Recent (1992 October) broad-band polarization measurements by J. H. Hough, J. A. Bailey, S. Young, & B. J. Wills show no significant changes since our original measurements, also suggesting that the polarization does not arise from the synchrotron mechanism.

5.3. *Scattering*

Scattering by small grains or electrons can produce very high, wavelength-independent polarization, approaching 100% for favorable geometries. There are several arguments in favor of a scattering origin for the polarization in IRAS 09104+4109: the high degree of polarization after correction for dilution by unpolarized emission lines and starlight, the angle of polarization being perpendicular to the direction of a possible collimated photoionizing continuum (§ 6.1), and the characteristic ultraviolet excess. A single scattering region with an effective optical depth less than unity is favored by the high degree of polarization and by the wavelength-independent polarization position angle. The high polarization alone suggests a geometry with a restricted range of scattering angles, and a large angle between our line of sight and the beam incident on the scatterers.

6. A SCATTERING MODEL

Three lines of evidence together lead us to conclude that IRAS 09104+4109 does, as originally suggested by K88, indeed contain a luminous, buried quasar, and that this is made visible by scattered nuclear light. We next discuss this evidence (§ 6.1, 6.2, 6.3), and details of the geometry are described in § 6.4.

6.1. *Extended* [O III] *Emission and the Polarization Position Angle*

The polarization position angle seems unrelated to the radio axis ($\Delta\theta \approx 56°$), but it is nearly perpendicular ($\Delta\theta \approx 84°$) to the position angle defined by the [O III] and R-band emission

extending $\sim 4''$ (14 kpc) from the nucleus (K88; Hutchings & Neff 1988). This relation between the [O III] and polarization position angles might be expected if the extended [O III] emission region is actually an "ionization cone" like those seen in many Seyfert galaxies (e.g., Pogge 1989; Fig. 4 of Pogge & De Robertis 1993), indicating that nuclear light is able to escape in the cone direction and is available for scattering.

6.2. *The Ionizing Continuum*

K88 observed the nuclear emission-line spectrum, but their slit also covered the extended nebulosity (as seen in their [O III] image): "Relative to [O III] λ5007, [O II] is stronger by a factor of 5, and Hβ is weaker by a factor of 2 at the secondary peak that at the nucleus." Using their measured fluxes for the nucleus gives the very high line intensity ratios [O III] λ5007/Hβ = 24 and [O II] λ3727/Hβ = 18 for the extended nebulosity, strongly suggesting that the extended [O III] region is indeed photoionized by a powerful nonthermal ultraviolet continuum. (See, for example, the line-ratio diagrams by Veilleux & Osterbrock 1987 and Pogge's 1989 spectra of extended [O III] emission in several Seyfert 1 and Seyfert 2 galaxies). In our scattering picture, the extended region seen in [O III] emission is photoionized gas, not necessarily a remnant of a captured galaxy as suggested by K88.

6.3. *The Scattered-Light Spectrum*

After correction for galaxy starlight and the strong narrow emission lines, the spectrum appears to have characteristics of a low-luminosity quasar—a continuum with $F_\nu \propto \nu^{-0.6}$, broad Mg II emission with typical quasar equivalent width ($\sim$38 Å) but with $M_v \sim -21.3$ (using data from Fig. 2, the Véron-Cetty & Véron 1991 conversion, and $h = 1$). The spectrum shape suggests little reddening, although this could be misleading if there is a mixture of scattered and reddened light.

The equivalent width of the nuclear narrow lines relative to the galaxy-subtracted continuum is more than a factor of 20 greater than the largest values observed in typical radio-loud quasars (1700 Å compared with, say, 85 Å, for [O III] λ5007), suggesting that we observe less than 5% of the true nuclear quasar luminosity of $M_v < -24.5$. The lack of obvious reddening suggests that the quasar nucleus is not simply heavily obscured. The high, approximately wavelength-independent degree of polarization and the relation of the polarization position angle to the extended [O III] morphology therefore lead us to conclude that a luminous quasar ($M_v < -24.5$) is buried in the nucleus of this galaxy, being revealed only in scattered light. We therefore predict that the broad Mg II emission will be found to be about 18% polarized. Broad, polarized Balmer emission should also be present. We find no evidence for broad, polarized Hβ emission in our low signal-to-noise polarized flux density spectrum. If we assume typical Hβ equivalent widths for quasars (e.g., Grandi 1981), we would be unable to detect polarized Hβ broader than ~ 3000 km s^{-1}.

The scattering region could be associated with the *R*-band extension (Hutchings & Neff 1988). However, the *R*-band extension can probably be accounted for by the strong [O III] emission within the *R* passband. Ultraviolet imaging is needed to investigate the scattering region further.

6.4. *Details of the Scattering Geometry*

In some Seyfert galaxies the extended [O III] emission is biconical, but in others the presence of a single "cone" implies that light from the far cone is blocked from view (e.g. Pogge 1989; Storchi-Bergmann, Wilson, & Baldwin 1992; Goodrich 1993). The [O III] emission appears to be one-sided in IRAS 09104+4109, which suggests that the system is tilted so that the far cone is obscured.

To further constrain the scattering geometry, we adopt the formalism of Brown & McLean (1977) to describe the emergent polarization from a single uniformly filled, optically thin scattering cone with opening half-angle θ_c, with axis inclined at an angle i to the line of sight, and illuminated by a hidden point source at the apex.

The fractional polarization[6] is given by

$$p_s = \frac{(3\gamma - 1)\sin^2 i}{2(1+\gamma) + (1-3\gamma)\sin^2 i},$$

where

$$\gamma = \frac{1}{3}\left(\frac{1-\mu_c^3}{1-\mu_c}\right)$$

and $\mu_c = \cos\theta_c$.

Since we measure the emergent polarization, we can invert the equation to investigate the possible combinations of i and θ_c that produce the observed p_s. Figure 5 shows the inclination i of the scattering cone as a function of the cone half-opening angle θ_c for constant emergent polarization p_s. The heavy contour represents the dilution-corrected polarization $\langle p \rangle \approx 18\%$. Since we do not see the central source directly, the only allowed values of i and θ_c are above the diagonal ($i - \theta_c > 0$). For $p_s = 18\%$, we find that there are two allowed regimes:

$$0 < \theta_c \lesssim 39^\circ, \quad 34 \lesssim i \lesssim 39^\circ$$

[6] Note that p_s in the first equation differs by a minus sign from that in Wills et al. (1992b). We reverse the sign conventions used by Brown & McLean (1977); the scattered light polarized perpendicular to the incident beam has positive polarization.

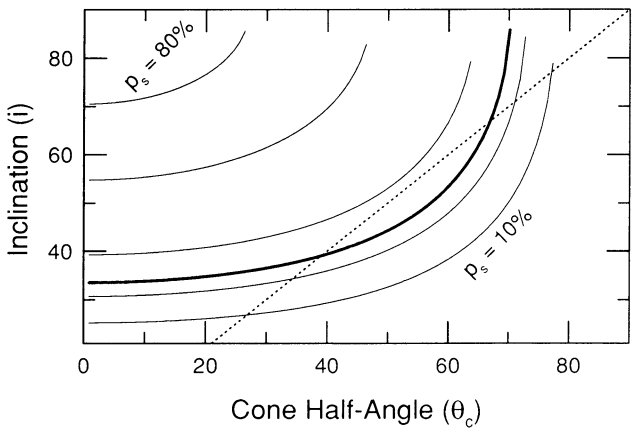

FIG. 5.—Results of calculations of optically thin scattering models assuming a uniformly filled cone with point-source illumination at the apex. Plotted are contours of constant polarization as a function of cone half-opening angle and inclination to the line of sight (in degrees). The heavy contour ($p_s = 18\%$) indicates the error-weighted average polarization after correction for dilution (see text). The contours correspond to $p_s = 10\%$, 15%, 18%, 25%, 50%, and 80%. The diagonal line represents $i = \theta_c$, where our line of sight allows us to just see the source at the apex. For IRAS 09104+4109 we do not see the central source directly, so we are restricted to the portion of the graph that is above and to the left of the diagonal.

or

$$66 \lesssim \theta_c \lesssim 71^\circ , \quad 67 \lesssim i \lesssim 90^\circ .$$

The morphology of the extended [O III] image suggests that $\theta_c < 50^\circ$, so we find the former possibility the more likely. (This morphological argument would be incorrect if the extent of the [O III] emission is determined by the geometry of the gas clouds rather than the illumination.) Even for polarizations of the order of our U-band measurement $p_s \sim 21\%$, the inclination of the scattering region cannot be large ($i \lesssim 40^\circ$). Interestingly, similar cone angles of $\sim 30^\circ$–60° have been derived for ionization or scattering cones in other AGNs (Pogge & De Robertis 1993; Unger et al. 1992; Wills et al. 1992b; Wilson, Ward, & Haniff 1988; Hutchings & Neff 1989).

We can also constrain θ_c by considering the infrared properties of IRAS 09104+4109. The strong near to mid-infrared emission probably arises from dust heated by the same obscured, nonthermal ultraviolet continuum that gives rise to the scattered light and ionizes the nuclear [O III] and the extended [O III] region. Thus the dust must not completely cover the source. K88 assume that the emission-line region is unreddened and calculate a dust covering factor $C_{\rm dust} \sim 0.98$ by comparing the Lyman continuum photons (via Hβ) with those required to heat the dust. This implies a cone half-angle

$$\theta_c \leq \cos^{-1}(2C_{\rm dust} - 1) = 16^\circ ,$$

and a corresponding inclination $i \sim 35^\circ$. For a given covering factor, this is an upper limit for θ_c, since there are probably other holes in the dust, e.g., where the radio jets escape. We can invert the argument and use our likely ranges for θ_c to constrain the covering factor, 0.98–0.89 and 0.70–0.66, for the two regimes.

In summary, the polarization, extended [O III] (and R-band) emission, and mid-infrared emission can be explained by a model in which a quasar nucleus is obscured from direct view by dust that covers $\sim$90%–98% of the source. A hole in the dust allows the quasar light to escape and photoionize a "cone" of gas with half-angle $\theta_c \lesssim 39^\circ$ and inclined by $i \sim 35^\circ$ to the line of sight. A few percent of the quasar light is scattered into the line of sight and thus polarized.

7. DISCUSSION

IRAS 09104+4109 is important, first, as an example of a luminous QSO whose dust-enshrouded nucleus is revealed in scattered light. Second, because it is the dominant cD galaxy in a rich cluster, it is important for the clues that it might offer concerning the influence of environment on the evolution of active nuclei. We discuss these issues below.

7.1. *Unified Schemes*

Unified schemes explain AGNs of different optical classes as a single type but differing in the dust covering (Rowan-Robinson 1977), or, more specifically, as a continuum and broad-line region (BLR) surrounded by an optically thick dusty torus, viewed at different inclinations (for reviews see Antonucci 1992, 1993). For low-luminosity AGNs, Seyfert 1 nuclei are viewed pole-on, while the Seyfert 2 nuclei, with weaker featureless continua and no obvious broad lines, are viewed at lower latitudes. Broad-line radio galaxies and narrow-line radio galaxies (NLRGs) are the radio-loud counterparts. For high-luminosity AGNs, QSOs (and the radio-loud quasars) are seen pole-on, while some radio galaxies may be quasars viewed at larger inclinations (Scheuer 1987; Barthel 1989).

A puzzle, even before modern unified schemes, was the dearth of QSO 2's—the high-luminosity counterparts of the Seyfert 2 galaxies and narrow-line radio galaxies. One explanation is that dust content, and hence dust covering, decreases with increasing luminosity (e.g., Malkan 1984; Miller & Goodrich 1990); perhaps there is a much thinner torus, as has been proposed to explain the scattered-light spectrum of OI 287 (0752+258; Goodrich & Miller 1988). On the other hand, a more natural explanation may be in terms of selection biases. Standard QSO search techniques using emission-line strength (grism and objective-prism searches), and color selection would miss reddened and obscured nuclei buried in distant faint host galaxies. There are four ways in which such hidden QSOs can be revealed (Antonucci 1993), and all four apply to IRAS 09104+4109. These are by means of (1) luminous, high-ionization narrow-line emission, (2) polarized continuum (and broad-line) emission that has been scattered from dust or electrons, (3) high infrared luminosities from the torus dust at equilibrium temperatures of $\sim$100 to $\sim$1000 K ($\lambda_{\rm max} \sim 3$–30 μm), and (4) high radio luminosity—at least for the few percent of AGNs that are radio-loud. IRAS 09104+4109 is the most luminous hidden QSO, but there are others (IRAS 20460+1925 and IRAS 23060+0505: Kay & Miller 1989; Hough et al. 1991; Hines 1991; Nakajima, Carleton, & Nishida 1991; IC 5063: Inglis et al. 1993; IRAS 110548−1131: Young et al. 1993a; IRAS 05189−2524: Wills & Hines 1993; Young et al. 1993b). The radio-quiet, distant ($z = 2.28$) galaxy IRAS F10214+4724 is potentially an even more extreme example—more luminous than any known QSO and with *white*-light polarization of 16% (Lawrence et al. 1993).

Finally, we have noted that IRAS 09104+4109 is the most luminous radio source to be associated with an ultraluminous *IRAS*-discovered AGN. As a radio galaxy, it may be compared with the 12 high- and intermediate-redshift radio galaxies investigated by Tadhunter et al. (1992; see also di Serego Alighieri, Cimatti, & Fosbury 1993 and references therein). They find that five of seven objects with $z > 0.5$ show high polarization ($p = 5\%$–20%), while no high-polarization objects were found in the range $0.2 < z < 0.5$, and they suggest that the implied redshift dependence is largely a consequence of the wavelength-dependent dilution of the polarization by starlight. In Figure 6 we have replotted the data from Tadhunter et al. (1992) to show the variation of polarization with rest wavelength rather than redshift. We include additional data as noted in the caption. The heavy line shows the observed wavelength dependence for IRAS 09104+4109. We also show the same polarization divided by 2, as a dotted curve. The wavelength dependence of polarization that we attribute to dilution by narrow emission lines and starlight represents the trends for radio galaxies quite well and supports the Tadhunter et al. hypothesis. The high-polarization sources are all classical FR II radio sources with polarization position angle nearly perpendicular to the radio axis (their Fig. 2). The fact that a polarized scattering region has actually been resolved in two of these objects (3C 386 and PKS 2152−69) and that the polarization position angle is perpendicular to the extended UV images in three high-redshift radio galaxies (3C 265, 3C 368, and 3C 277.2) suggests that this mechanism and geometry apply more generally. Thus Tadhunter et al. suggest that the high polarization and alignment are due to light from a hidden AGN escaping along the radio axis, and scattered into the line of sight.

IRAS 09104+4109 appears to be an interesting exception to

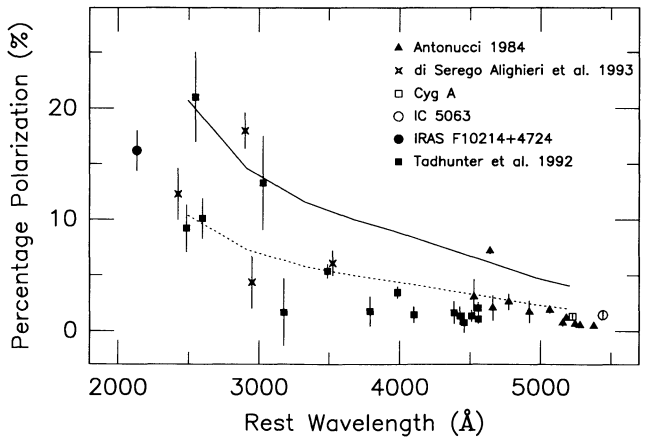

FIG. 6.—Polarization as a function of rest wavelength for radio galaxies. The solid line connects the observed broad-band data for IRAS 09104+4109. The dashed line shows the same, but with percentage polarization divided by 2, for easier comparison with the trend shown by the other data. See Antonucci (1984), Tadhunter et al. (1992), di Serego Alighieri et al. (1993), and Inglis et al. (1993) for references to data.

the polarization–radio-structure alignment noted in other high-luminosity radio galaxies.

7.2. *Evolution of AGNs in Galaxy Clusters*

Besides the misalignment (§ 7.1), other radio properties of IRAS 09104+4109 present an interesting anomaly. The radio structure appears to be that of a classic (FR II) double-lobed source, having a strong barely resolved nuclear core, well-collimated bridges (jets), and apparently well-defined hot spots (or edge-brightened lobes; the linear resolution is not sufficient to be sure) collinear with the core. However, in other ways the classification is not quite clear: IRAS 09104+4109 is borderline in radio luminosity between the FR I and more luminous FR II sources. The low sidedness ratio (i.e., the prominence of the counterjet) is very unusual for a FR II source, especially one of this relative core strength ($R \sim 1$), and, if the jets are relativistically beamed, it indicates that the extended structure lies very close to the sky plane. Usually the core spectra and hot spot spectra are flatter ($\alpha \sim 0$) than we find for IRAS 09104+4109; the spectral indices for IRAS 09104+4109 are more like those found in FR I sources. The unusual radio structure could be explained by a decoupling of the nuclear and large-scale jet directions such that the nuclear jet is no longer in the sky plane but is beamed at a smaller inclination angle. This could also explain the anomalous optical alignment: the ionizing continuum and prescattered light escape the nucleus at a projected position angle of 40° to the northwest radio jet. Our analysis suggests that the scattering cone's axis is inclined at $\sim$35° to the line of sight; if the radio core is beamed, this is probably within 20°–30° of the line of sight (Hough & Readhead 1989). We propose that there has been a recent change in jet direction and that a nuclear radio jet, beamed at a new, intermediate inclination, has blasted a new hole in the obscuring material, allowing the hard central continuum radiation to escape. The radio spectrum of the old beam and hot spots steepen, as their power is no longer replenished. This may be a more general phenomenon in cluster radio sources where very steep low- and high-frequency radio spectra are observed (Slingo 1974). The relatively small inclination angle of the new jet could explain why we do not see a far-side radiation cone.

The relation of the radio source to the dominant cD galaxy in a particularly rich cluster ($z = 0.442$) is potentially very interesting. The cD galaxy associated with IRAS 09104+4109 is of typical luminosity and size for a giant dominant cluster galaxy (K88). These extreme characteristics are thought to arise through cannibalism of inner cluster members, and, at least in the case of luminous radio galaxies, this supplies the fuel and angular momentum for an AGN. Hutchings & Neff's (1988) images show some evidence for very nearby companions, although they claim that there is no evidence for interaction or merging. Similarly, Sanders et al. (1988) find evidence for interactions with companion galaxies in nearly all *IRAS* ultraluminous galaxies, and the extreme infrared luminosity is suggested to arise from dust within a few hundred parsecs of the nucleus that is heated by the newly fueled central engine.

FR II radio galaxies often inhabit rich clusters at $z \sim 0.5$, but almost totally avoid them at low z. But FR I radio galaxies are typically found in less rich clusters both at $z \sim 0$ and at $z = 0.5$ (Hill & Lilly 1991). Hill & Lilly suggest the possibility that FR II sources were favored at $z \sim 0.5$ because the pressure of the intergalactic medium was lower in some clusters at earlier epochs. An increase in pressure of the intergalactic medium in clusters since $z \sim 0.5$ may disrupt the jets in FR II sources by present epochs—a suggestion that has some support from models of cluster evolution.

For IRAS 09104+4109, these ideas are of special interest when we recognize that the radio axis, which, we argued above, lies in the sky plane, *appears quite accurately aligned with the minor axis of the rich, flattened cluster* (position angles 333° and 340° $\pm$ 4°, respectively). If the central engine is fueled by galaxies in the plane of the cluster, its net angular momentum would probably be along the cluster minor axis, resulting in the observed good alignment with the radio jet. The fact that a well-defined FR II–like *collinear* structure has propagated and survived may be related to lower gas pressures in directions away from the plane of the cluster. This geometry also favors our supposition that the jets lie close to the sky plane.

The recent change in jet direction proposed above may signal the demise of the FR II radio source as it evolves to type FR I along with increasing pressure of the intracluster medium.

Having deduced that IRAS 09104+4109 is in fact a luminous buried quasar, we find it anomalous in yet another respect. Although we find it to be a radio-loud FR II radio source at 178 MHz according to the luminosity criterion of Fanaroff & Riley (1974), because of its steep radio spectrum and enormous infrared luminosity, it may actually fall into the radio-quiet class using the definitions of "radio-quiet" at high frequencies (Kellermann et al. 1989; Visnovsky et al. 1992). At a rest frequency of 178 MHz we find a luminosity $\sim 7.4 \times 10^{24}$ W Hz^{-1} sr^{-1}, just above the 5×10^{24} cutoff. Near 8 GHz, the (isotropic) luminosity is $\sim 5 \times 10^{23}$ compared with the cutoff of 2.5×10^{24} W Hz^{-1}. Another criterion, the ratio r of radio luminosity at 5 GHz rest frequency to optical luminosity (B band), can be calculated assuming that the infrared luminosity is powered by a normal optical-UV accretion disk. If we could see that continuum, then, given a range of accretion disk fits to standard luminous QSO continua (Laor & Netzer 1989), the B band (rest frame) should appear as bright as 16.8 to 15.1 mag, with $r = 3.7$–17. These values may be compared with the range 0.1–1 for radio-quiet QSOs, and 10 to above 100 for radio-loud

quasars. Now IRAS 09104+4109 provides an interesting comparison with the remarkable QSO E1821+643 (Lacy, Rawlings, & Hill 1992). This X-ray–discovered QSO is extremely luminous optically, is also borderline radio-quiet, and is the dominant cD galaxy in a particularly luminous cluster ($z = 0.297$). The interest is that, like IRAS 09104+4109, its environment, the center of a rich cluster at $z < 0.5$, is thought to be the exclusive domain of radio-loud AGNs. IRAS 09104+4109 may be intrinsically like E1821+643, but viewed at a different angle.

8. SUMMARY

IRAS 09104+4109 shows strong wavelength-dependent polarization ranging from 4% at 7500 Å to 21% at 3600 Å, while the position angle is wavelength-independent within $\sim 5°$. Our spectropolarimetry shows that the narrow emission lines are unpolarized. After correction for dilution by the unpolarized host galaxy continuum and emission lines, we find that the nuclear continuum rises into the UV and has $\langle p \rangle \approx 18\%$ independent of wavelength (within quite large uncertainties). We also detect a broad component of the Mg II λ2798 emission line, with width 10,000 km s^{-1} (FWHM) and equivalent width 38 Å typical of quasars. The most plausible polarization mechanism is scattering by small dust grains or electrons. The polarization position angle ($\sim 97°$) is almost perpendicular to the position angle ($\sim 14°$) of the high-ionization [O III] region extending from the galaxy nucleus. A plausible picture is therefore one in which QSO continuum radiation is able to escape through a region of low dust cover, ionizing gas in that direction and scattering into the line of sight. Thus we predict that the broad component of Mg II will be highly polarized, with $p \sim 18\%$. Calculations, assuming an intrinsic degree of polarization $\sim 18\%$ and an optically thin cone of scatterers with the nucleus as origin, indicate a cone with half–opening angle of less than 39° tilted at $\sim 35°$ to the observer. The existence of such hidden luminous AGNs suggests that QSO 2's—the missing high-luminosity counterparts of Seyfert 2 nuclei and narrow-line radio galaxies—may not be rare as previously supposed but have simply been missed in searches for QSOs that are biased against the faint reddened nuclei of distant galaxies.

IRAS 09104+4109 is the most distant and most luminous known radio-loud *IRAS*-discovered AGN. Its observed wavelength dependence of polarization represents quite well the redshift dependence of polarization for radio galaxies noted by Tadhunter et al. (1992), supporting their suggestion that this is a result of observing shorter rest wavelengths at higher redshifts. Compared with other radio galaxies, IRAS 09104+4109 is anomalous in the misalignment of the polarization position angle and radio-structure axis. Such misalignments may be more common in the luminous quasars where low-level polarization is not always perpendicular to radio structure, and where inner and outer radio structure are often not aligned.

IRAS 09104+4109 is a classic double radio source of luminosity intermediate between types FR I and FR II, but it defies classification as either. The well-collimated jets and hot spots are characteristic of FR II sources, but the prominent counterjet and steep spectral indices are not. This suggests that the large-scale structure lies near the plane of the sky, but core dominance suggests an inner structure axis beamed closer to the line of sight. We propose that the optical-UV radiation cone is aligned with an inner radio jet. This could be confirmed with VLBI observations.

IRAS 09104+4109 is the central cD galaxy in a rich, flattened galaxy cluster at a redshift of 0.442. The extended radio jets are perpendicular to the major axis of the cluster. We suggest that the angular momentum of the central engine is derived from that of captured galaxies in the cluster plane, and the persistence of the well-collimated jets may derive from the lower pressures outside the cluster plane. We also suggest that the recent misalignment of the radio jet and radiation cone with respect to the extended radio jets may represent the evolution to FR I structure seen between epochs of $z = 0.5$ and the present in a statistical study of radio galaxy environments by Hill & Lilly (1991).

We thank Derek Wills for help during the 1989 January and April observations, and Don Hamilton for sending us the red spectrum data from K88. Thanks are also due to R. W. Goodrich for his retrofitting of the LCS with spectropolarimetry optics and for his help with the VISTA data reduction. We thank D. Doss and E. Dutchover for excellent maintenance and operation of the instruments. D. Hines wishes to thank Stefani Hines for her strong support. Thanks to G. Hill, D. Wills, and D. H. Hough for many helpful discussions. This work was supported in part by NSF grant AST-8714937 to B. and D. Wills, and modification of the spectrograph for spectropolarimetry was supported by the University of Texas University Research Institute grant URI R-154 and a Summer Research Award to B. J. W.

REFERENCES

Antonucci, R. R. J. 1984, ApJ, 278, 499
———. 1992, in Testing the AGN Paradigm, ed. S. S. Holt, S. G. Neff, & C. M. Urry (New York: AIP), 486
———. 1993, ARA&A, 31, 473
Barthel, P. D. 1989, ApJ, 336, 606
Breger, M. 1979, ApJ, 233, 97
Bridle, A. H., & Perley, R. A. 1984, ARA&A, 22, 319
Brindle, C., Hough, J. H., Bailey, J., Ward, M. J., Axon, D. J., Sparks, W. B., & McLean, I. S. 1990a, MNRAS, 244, 577
———. 1990b, MNRAS, 244, 604
Brown, J. C., & McLean, I. S. 1977, A&A, 57, 141
Burstein, D., & Heiles, C. 1982, AJ, 87, 1165
di Serego Alighieri, S., Cimatti, A., & Fosbury, R. A. E. 1993, ApJ, 404, 584
Fanaroff, B. L., & Riley, J. M. 1974, MNRAS, 167, 3P
Goodrich, R. W. 1991, PASP, 103, 1314
———. 1993, ApJ, 399, 50
Goodrich, R. W., & Miller, J. S. 1988, ApJ, 331, 332
Grandi, S. A. 1981, ApJ, 251, 451
Hill, G. J., & Lilly, S. J. 1991, ApJ, 367, 1
Hines, D. C. 1991, ApJ, 374, L9
Hines, D. C., & Wills, B. J. 1993, in preparation
Hough, D. H., & Readhead, A. C. S. 1989, AJ, 98, 1208
Hough, J. H., Brindle, C., Wills, B. J., Wills, D., & Bailey, J. A. 1991, ApJ, 372, 478
Hsu, J.-C., & Breger, M. 1982, ApJ, 262, 732
Hutchings, J. B., & Neff, S. G. 1988, AJ, 96, 1575
———. 1989, AJ, 97, 1306
Impey, C. D., Lawrence, C. R., & Tapia, S. 1991, ApJ, 375, 46
Inglis, M. D., Brindle, C., Hough, J., Young, S., Axon, D., Bailey, J., & Ward, M. 1993, MNRAS, in press
Kay, L. E., & Miller, J. S. 1989, BAAS, 21, 1099
Kellermann, K. I., Sramek, R., Schmidt, M., Shaffer, D. B., & Green, R. 1989, AJ, 98, 1195
Kleinmann, S. G., Hamilton, D., Keel, W. C., Wynn-Williams, C. G., Eales, S. A., Becklin, E. E., & Kuntz, K. D. 1988, ApJ, 328, 161 (K88)
Kleinmann, S. G., & Keel, W. C. 1987, in Star Formation in Galaxies, ed. Carol J. Lonsdale Persson (NASA CP-2466), 559
Lacy, M., Rawlings, S., & Hill, G. 1992, MNRAS, 258, 828
Laor, A., & Netzer, H. 1989, MNRAS, 238, 897
Lawrence, A., et al. 1993, MNRAS, 260, 28

Malkan, M. A. 1984, in X-Ray and UV Emission from Active Galactic Nuclei, ed. W. Brinkman & J. Trumpler (MPE Rep., No. 184; Garching: Max-Planck-Institut für Physik und Astrophysik), 121
Martin, P. G., Thompson, I. B., Maza, J., & Angel, J. R. P. 1983, ApJ, 266, 470
Miller, J. S., & Goodrich, R. W. 1990, ApJ, 355, 456
Miller, J. S., Robinson, L. B., & Goodrich, R. W. 1988, in Instrumentation for Ground-based Astronomy, ed. L. B. Robinson (New York: Springer-Verlag), 157
Nakajima, T., Carleton, N., & Nishida, M. 1991, ApJ, 375, L1
Pogge, R. W. 1989, ApJ, 345, 730
Pogge, R. W., & De Robertis, M. M. 1993, ApJ, 404, 563
Rowan-Robinson, M. 1977, ApJ, 213, 635
Sanders, D. B., Soifer, B. T., Elias, J. H., Madore, B. F., Matthews, K., Neugebauer, G., & Scoville, N. Z. 1988, ApJ, 325, 74
Scheuer, P. 1987, in Superluminal Radio Sources, ed. J. Zensus & T. Pearson (Cambridge: Cambridge Univ. Press), 104
Serkowski, K., Mathewson, D. E., & Ford, V. 1975, ApJ, 196, 261
Simmons, J. F. L., & Stewart, B. G. 1985, A&A, 142, 100
Slingo, A. 1974, MNRAS, 168, 307
Stockman, H. S., Moore, R. L., & Angel, J. R. P. 1984, ApJ, 279, 485
Stone, R. P. S. 1977, ApJ, 218, 767
Storchi-Bergmann, T., Wilson, A. S., & Baldwin, J. A. 1992, ApJ, 396, 45
Tadhunter, C. N., Scarrott, S. M., Draper, P., & Rolph, C. 1992, MNRAS, 256, 53P
Thompson, I. B., & Martin, P. G. 1988, ApJ, 330, 121
Unger, S. W., Lewis, J. R., Pedlar, A., & Axon, D. J. 1992, MNRAS, 258, 371
Veilleux, S., & Osterbrock, D. E. 1987, ApJS, 63, 295
Véron-Cetty, M.-P., & Véron, P. 1991, A Catalogue of Quasars and Active Nuclei (ESO Sci. Rep., No. 10; 5th ed.; Garching: ESO)
Visnovsky, K. L., Impey, C. D., Foltz, C. B., Hewett, P. C., Weymann, R. J., & Morris, S. L. 1992, ApJ, 391, 560
Wardle, J. F. C., & Kronberg, P. P. 1974, ApJ, 194, 249
Wells, D. C. 1978, Integrated Spectral Energy Distributions of Galaxies (Univ. Texas Pub. Astron., No. 13; Austin: Univ. Texas)
Whittet, D. C. B., Martin, P. G., Hough, J. H., Rouse, M. F., Bailey, J. A., & Axon, D. J. 1992, ApJ, 386, 562
Wills, B. J., & Hines, D. C. 1993, ApJ, in preparation
Wills, B. J., Wills, D., Breger, M., Antonucci, R. R. J., & Barvainis, R. 1992a, ApJ, 398, 454
Wills, B. J., Wills, D., Evans, N. J., Natta, A., Thompson, K. L., Breger, M., & Sitko, M. L. 1992b, ApJ, 400, 96
Wilson, A. S., Ward, M. J., & Haniff, C. A. 1988, ApJ, 334, 121
Young, S., Hough, J. H., Bailey, J. A., Axon, D. J., & Ward, M. J. 1993a, MNRAS, 260, 1P
Young, S., et al. 1993b, MNRAS, in preparation